CHEMISTRY
A EUROPEAN JOURNAL

DOI: 10.1002/chem.200903588

Double C–H Activation of Ethane by Metal-Free $SO_2^{\bullet+}$ Radical Cations

Giulia de Petris,*[a] Antonella Cartoni,[a] Anna Troiani,[a] Vincenzo Barone,[b] Paola Cimino,[c] Giancarlo Angelini,[d] and Ornella Ursini[d]

Abstract: The room-temperature C–H activation of ethane by metal-free $SO_2^{\bullet+}$ radical cations has been investigated under different pressure regimes by mass spectrometric techniques. The major reaction channel is the conversion of ethane to ethylene accompanied by the formation of $H_2SO_2^{\bullet+}$, the radical cation of sulfoxylic acid. The mechanism of the double C–H activation, in the absence of the single activation product HSO_2^+, is elucidated by kinetic studies and quantum chemical calculations. Under near single-collision conditions the reaction occurs with rate constant $k = 1.0 \times 10^{-9}$ ($\pm 30\,\%$) $cm^3 s^{-1} molecule^{-1}$, efficiency = 90 %, kinetic isotope effect $k_H/k_D = 1.1$, and partial H/D scrambling. The theoretical analysis shows that the interaction of $SO_2^{\bullet+}$ with ethane through an oxygen atom directly leads to the C–H activation intermediate. The interaction through sulfur leads to an encounter complex that rapidly converts to the same intermediate. The double C–H activation occurs by a reaction path that lies below the reactants and involves intermediates separated by very low energy barriers, which include a complex of the ethyl cation suitable to undergo H/D scrambling. Key issues in the observed reactivity are electron-transfer processes, in which a crucial role is played by geometrical constraints. The work shows how mechanistic details disclosed by the reactions of metal-free electrophiles may contribute to the current understanding of the C–H activation of ethane.

Keywords: C–H activation · ethane · mass spectrometry · radical ions · sulfur

Introduction

The heart of the matter in the current exploitation of available resources is the conversion of alkanes into different functionalized compounds. Several approaches have been pursued in decades of active research on this thorny problem; on the whole, effective C–H activation steps are required to achieve high rates of reaction and selectivities. The first studies succeeded using metal-free electrophiles in strong acid media, thereafter the electrophilic activation was investigated both in strong acids and in the gas phase.[1] Only a limited number of metal-free electrophiles have been studied over the years,[1i–j,2] and our current knowledge of C–H electrophilic activation largely rests on a great deal of detailed experimental and theoretical studies of the reactivity of bare and ligated metal ions.[3]

Recently, the first metal-free oxides to effectively activate methane have been reported: the $SO_2^{\bullet+}$[4a] and $P_4O_{10}^{\bullet+}$[5] electrophiles, both oxygen-centered radicals. Activation by these species is in line with recent analyses of the main factors that affect the electrophilic activation of hydrocarbons—the spin density of charged reactants[3m] and the radical-cationic character developed in transition states and intermediates.[1i–j] Charge-transfer processes are also relevant to the mechanism of the C–H activation. For example, the C–H bond of the alkane may be elongated by inner-sphere electron transfer to the electrophile, which leads to an incipient radical carbocation, or the electron may be coupled to the hydrogen atom that is directly transferred.[1j]

These effects can be better investigated with $E^{\bullet+}$ electrophiles, in which charge and spin are separated, as typically

[a] Prof. Dr. G. de Petris, Dr. A. Cartoni, Dr. A. Troiani
Dipartimento di Chimica e Tecnologie del Farmaco
Università "La Sapienza", P. le Aldo Moro 5, 00185 Roma (Italy)
Fax: (+39) 6-49913602
E-mail: giulia.depetris@uniroma1.it

[b] Prof. Dr. V. Barone
Scuola Normale Superiore di Pisa
Piazza dei Cavalieri 7, 56126 Pisa (Italy)

[c] Dr. P. Cimino
Dipartimento di Scienze Farmaceutiche
Università degli Studi di Salerno
Via Ponte Don Melillo, 84084 Fisciano (SA) (Italy)

[d] Dr. G. Angelini, Dr. O. Ursini
Istituto di Metodologie Chimiche
Area della Ricerca di Roma del CNR, CP 10
00016 Monterotondo Stazione (RM) (Italy)

Supporting information for this article is available on the WWW under http://dx.doi.org/10.1002/chem.200903588.

occurs in metal-oxo ions or metal-free oxides $SO_2^{\bullet+}$ and $P_4O_{10}^{\bullet+}$. Further insight can be gained from alkanes with ionization energies lower than that of the reactant. For instance, C_2H_6, unlike CH_4, has an ionization energy (11.52 eV) lower than that of SO_2 (12.35 eV).[6] The C–H activation of ethane, known from studies of transition-metal ions, occurs by single and double hydrogen-atom abstraction (to give EH^+ or $EH_2^{\bullet+}$) and by dehydrogenation and double dehydrogenation (to give $EC_2H_4^{\bullet+}$ or $EC_2H_2^{\bullet+}$).[7] Very recently, the scant information available on the reactivity of metal-free electrophiles with ethane[8] has been enriched by Schwarz et al., who reported on the polynuclear $P_4O_{10}^{\bullet+}$ ion.[9] This ion undergoes hydrogen-atom abstraction to give $[P_4O_9(OH)]^+$, with a rate constant of $1.1\times10^{-9}\,cm^3s^{-1}molecule^{-1}$ and a notable efficiency of almost 100%. The $SO_2^{\bullet+}$ radical cation is a promising candidate for further mechanistic studies along this line. We recently found that $SO_2^{\bullet+}$ activates the strong C–H bond of methane and the even stronger O–H bond of water.[4] The former occurs through the intermediate $[OSOH\cdots CH_3]^{\bullet+}$, which was detected experimentally,[4a] and the latter with the exceptional efficiency of 100%.[4b] We now report that the reaction of $SO_2^{\bullet+}$ with C_2H_6 effectively undergoes double hydrogen-atom abstraction to produce ethylene. The features of this reaction mechanism, studied under different pressure regimes, may be key to a deeper understanding of the C–H activation of ethane and related catalytic processes.

Results and Discussion

Experimental results: The room-temperature activation of ethane by $SO_2^{\bullet+}$ ions leads to double hydrogen-atom abstraction and generation of C_2H_4, both in the low- and high-pressure limit. The experiments performed under these conditions are illustrated below.

Low-pressure experiments: Experiments performed by Fourier-transform ion cyclotron resonance (FT-ICR) mass spectrometry, at the pressure of approximately 10^{-8} Torr, show that thermal $SO_2^{\bullet+}$ ions react with C_2H_6 to give $H_2SO_2^{\bullet+}$ and ethylene [Eq. (1)].

$$SO_2^{\bullet+} + C_2H_6 \rightarrow H_2SO_2^{\bullet+} + C_2H_4 \quad (1)$$

The single hydrogen-atom abstraction product HSO_2^+ is not formed, proven by experiments accurately performed in the absence of water (see the Experimental Section). These conditions must be met because HSO_2^+ is efficiently produced by the reaction of $SO_2^{\bullet+}$ with water, even in the presence of only trace amounts of background water.[4b] Accordingly, the absence of signals corresponding to HSO_2^+ and DSO_2^+ in experiments with C_2H_6 and C_2D_6, allows conclusive exclusion of this reaction channel.

In addition to $H_2SO_2^{\bullet+}$, the $C_2H_5^+$ and $C_2H_4^{\bullet+}$ ions are observed. The possible role of dissociative charge-transfer shown in Equations (2) and (3) will be addressed in the next paragraphs.

$$SO_2^{\bullet+} + C_2H_6 \rightarrow C_2H_5^+ + [H^{\bullet}+SO_2;\ HSO_2^{\bullet}] \quad (2)$$

$$SO_2^{\bullet+} + C_2H_6 \rightarrow C_2H_4^{\bullet+} + [H_2+SO_2] \quad (3)$$

Figure 1 shows the kinetic plot of the reactant decay and products growth. The following results are obtained from the kinetic study: rate constant $k=1.0\times10^{-9}$ $(\pm30\%)\,cm^3s^{-1}molecule^{-1}$, efficiency $k/k_{coll}=90\%$ (k_{coll} = collision rate), branching ratios: $H_2SO_2^{\bullet+}=53\%$, $C_2H_5^+=28\%$, $C_2H_4^{\bullet+}=19\%$. The overall kinetic isotope effect (KIE), measured by the reaction between $SO_2^{\bullet+}$ and C_2D_6, is $k_H/k_D=1.1$. In this reaction, the branching ratios $D_2SO_2^{\bullet+}=56\%$, $C_2D_5^+=31$, $C_2D_4^{\bullet+}=13\%$ suggest that the channel shown in Equation (3) is affected by the isotopic substitution and is mainly responsible for the small KIE observed. Consistent with this are the results from the reaction between $SO_2^{\bullet+}$ and CH_3CD_3, which yields the following products:

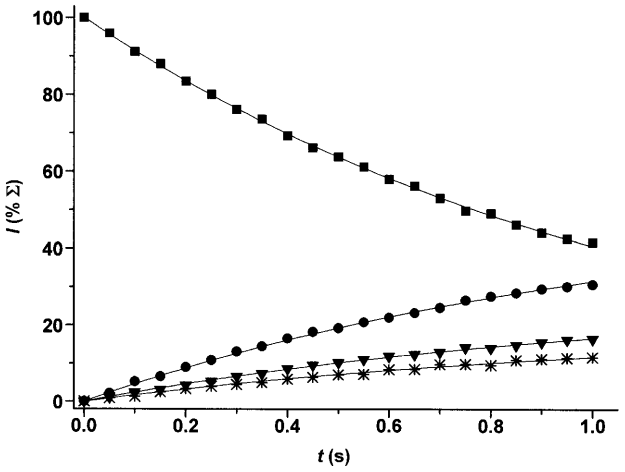

Figure 1. Kinetic plot and best-fit lines of the reaction of thermal $SO_2^{\bullet+}$ ions with C_2H_6 (FT-ICR). $P(C_2H_6)=2.7\times10^{-8}$ Torr. $SO_2^{\bullet+}$ ($R^2=0.999$) (■); $H_2SO_2^{\bullet+}$ ($R^2=0.999$) (●); $C_2H_5^+$ ($R^2=0.998$) (▼); $C_2H_4^{\bullet+}$ ($R^2=0.994$) (*).

$$SO_2^{\bullet+} + CH_3CD_3 \rightarrow HDSO_2^{\bullet+} + C_2H_2D_2\ (34\%) \quad (4a)$$

$$SO_2^{\bullet+} + CH_3CD_3 \rightarrow H_2SO_2^{\bullet+} + C_2HD_3\ (16\%) \quad (4b)$$

$$SO_2^{\bullet+} + CH_3CD_3 \rightarrow D_2SO_2^{\bullet+} + C_2H_3D\ (7\%) \quad (4c)$$

$$SO_2^{\bullet+} + CH_3CD_3 \rightarrow C_2H_2D_3^+ + [H^{\bullet}+SO_2,\ HSO_2^{\bullet}]\ (13\%) \quad (5a)$$

$$SO_2^{\bullet+} + CH_3CD_3 \rightarrow C_2H_3D_2^+ + [D^{\bullet}+SO_2,\ DSO_2^{\bullet}]\ (13\%) \quad (5b)$$

$$SO_2^{\bullet+} + CH_3CD_3 \rightarrow C_2H_2D_2^{\bullet+} + [HD+SO_2]\ (17\%) \quad (6a)$$

The measurement of the formation rate constant, relevant to the major channel [Eq. (1) (C_2H_6, C_2D_6) and Eq. (4) (CH_3CD_3)], confirms that this rate constant is not affected by the isotopic substitution: $k(1)$ (C_2H_6) and $k(4)$ (CH_3CD_3) $=5.3\times10^{-10}$ ($\pm30\%$) $cm^3s^{-1}molecule^{-1}$, $k(1)$ (C_2D_6) $=5.1\times10^{-10}$ ($\pm30\%$) $cm^3s^{-1}molecule^{-1}$. Nonetheless, the ratio of the products formed by reactions (4a), (4b), and (4c), 2.1:1.0:0.44, shows that the formation of hydrogen-containing ions is favored. This finding suggests the occurrence of some scrambling that, though non-rate-determining for the channel (4), does not lead to the statistical distribution (3:1:1). Importantly, only $C_2H_2D_2^{\bullet+}$ is formed by the channel (6a), whereas the ratio of the products formed by reactions (5a) and (5b) is 1.

High-pressure experiments: In these experiments, performed by ion-trap mass spectrometry (ITMS), the reaction occurs in a helium buffer gas, which typically ensures pressures of the order of mTorr.[10] In addition, water cannot thoroughly be eliminated from the apparatus, which may cause some $SO_2^{\bullet+}$ ion loss. Therefore, we carried out the kinetic study by performing an accurate calibration procedure to subtract the background contribution (see the Experimental Section). Figure 2A is an example of a background reaction profile, recorded before any experiment to obtain the pseudo-unimolecular rate constants (k_{obs}) of the $SO_2^{\bullet+}$ reaction with C_2H_6. These are reported in Figure 2B as a function of the neutral density. The time profiles (Figure 3) show that under high-pressure conditions $H_2SO_2^{\bullet+}$ is still the main product of the reaction with ethane. In addition, $C_2H_5^+$, $C_2H_4^{\bullet+}$, and very small signals corresponding to $C_2H_6^{\bullet+}$ are observed. The time profile of $C_2H_5^+$ is similar to that of HSO_2^+ (from the side reaction with water) because they both protonate water. As a consequence, at the longest reaction times only three ions are observed, namely, $H_2SO_2^{\bullet+}$, H_3O^+, and $C_2H_4^{\bullet+}$. Notably, no $[SO_2C_2H_6]^{\bullet+}$ reaction intermediate is observed at any point.

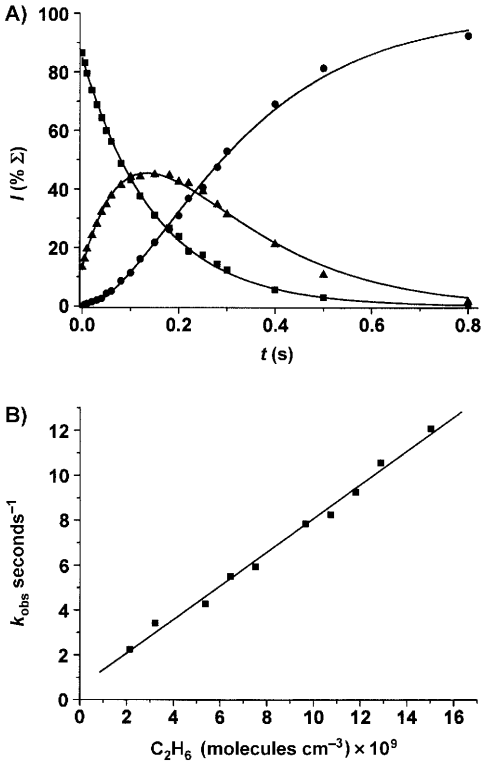

Figure 2. A) Kinetic plot and best-fit lines of the reaction of thermal $SO_2^{\bullet+}$ ions with background water (ITMS). $SO_2^{\bullet+}$ ($R^2=0.999$) (■); HSO_2^+ ($R^2=0.993$) (▲); H_3O^+ ($R^2=0.998$) (●). See ref. [4b] for the kinetic scheme, in which $[HSO_2^+]_{t=0}\neq0$. B) Plot of the corrected rate constants k_{obs} of the reaction between $SO_2^{\bullet+}$ and C_2H_6, as a function of C_2H_6 molecules cm^{-3} ($R^2=0.992$).

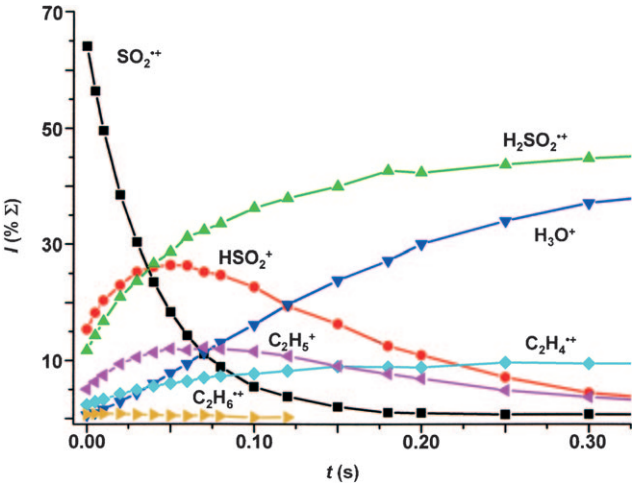

Figure 3. Time profiles of the reaction of thermal $SO_2^{\bullet+}$ ions with C_2H_6 (ITMS). $P(C_2H_6)=4.7\times10^{-7}$ Torr.

$SO_2^{\bullet+}$ decays according to first-order kinetics and the derived bimolecular rate constant, $k=8.6\times10^{-10}$ ($\pm30\%$) $cm^3s^{-1}molecule^{-1}$, is in reasonable agreement with that obtained at low pressure. Comparable differences have been observed with ICR and high-pressure selected-ion flow tube (SIFT) experiments.[3e] The branching ratios may only be approximately evaluated ($H_2SO_2^{\bullet+}=59\%$, $C_2H_5^+=28\%$, $C_2H_4^{\bullet+}=13\%$), whereas the ratio of the products $H_2SO_2^{\bullet+}$ and $C_2H_4^{\bullet+}$ can be accurately evaluated because these are not affected by consecutive reactions. The 4.6:1.0 ratio, measured for the reaction time of 4 s, shows that the formation of $C_2H_4^{\bullet+}$ is less than observed at low pressure.

Such a difference is traced to the greater collisional stabilization at high pressure (ITMS), compared with near single-collision conditions (ICR). Although the reaction is initiated by thermal $SO_2^{\bullet+}$ ions in both experiments, possible intermediates formed with excess energy are not effectively cooled in ICR, whereas the opposite is true in ITMS.[3e,11] For instance, the charge transfer is expected to produce $C_2H_6^{\bullet+}$ ions that subsequently undergo unimolecular dissociation to $C_2H_4^{\bullet+}$; this occurs more effectively at low pressure than at high pressure after termolecular stabilization. The occurrence of charge transfer to C_2H_6 is proved here by the detection of the small fraction of $C_2H_6^{\bullet+}$ that escapes dissociation up until the reactant ion disappears. Notably, the high overall pressure breaks that reaction channel, which is

affected by isotopic substitution in FT-ICR. Both effects may be related to the kinetic features of the formation of $C_2H_4^{\bullet+}$, which thus delineates a different path for the reactions shown in Equations (1)–(3).

In summary, the most salient features that emerge from all the above experimental results are as follows:

1) the reaction efficiency and the very small KIE, which point to a process that occurs without kinetic barriers.
2) the absence of HSO_2^+ as a product from the first C–H activation, in the presence of the double C–H activation product $H_2SO_2^{\bullet+}$.
3) the isotopic distribution of the products from the reaction of CH_3CD_3, which suggests the superimposition of H/D scrambling in the major reaction channel.
4) the effect of the overall pressure and isotopic substitution on the formation of $C_2H_4^{\bullet+}$.

Computational analysis: A detailed quantum mechanical (QM) investigation has been performed to identify the conceivable pathways for the reaction between $SO_2^{\bullet+}$ and C_2H_6. In particular, the analysis has focused on the C–H activation step and the reaction pathway leading to ethylene loss. Figures 4 and 5 report the minima identified on the $[SO_2C_2H_6]^{\bullet+}$ potential energy surface, relevant to C–H activation (**S1**, **O1a**, **O1**) and ethylene loss (**O2**, **O3**, **O4**), respectively. The transition state structures (**TS(S1–O1a)**, **TS(O1a–O1)**, **TS(O1–O2)**, **TS(O2–O3)**, **TS(O3–O4)**) are also reported in Figures 4 and 5. The formation enthalpies, geometrical parameters, atomic charges, and spin densities are reported in Tables 1 and 2. Table 3 reports the $\Delta H°$ values of the relevant dissociation reactions. Different conformers of **O1** and **O1a** have been found at slightly different energies; their geometries as well as their interconversion processes are reported in the Supporting Information.

The ions reported in Figure 4 can formally be denoted as $[SO_2\cdots C_2H_6]^{\bullet+}$ (**S1**) and $[HSO_2\cdots C_2H_5]^{\bullet+}$ (**O1a**, **O1)** species. **S1** is the only encounter complex that corresponds to an energy minimum and involves an interaction of the hydrogen atom of the alkane C_2H_6 with the sulfur atom of $SO_2^{\bullet+}$. The analogous interaction with the oxygen atom directly leads to hydrogen-atom transfer (see below). In **S1** the C–H bond is slightly elongated (1.222 Å) and charge and spin are equally distributed between SO_2 and C_2H_6. (Table 2). **S1** isomerizes to the $[HSO_2\cdots C_2H_5]^{\bullet+}$ complex **O1a** (by overcoming an energy barrier of 1 kcal mol^{-1}), in which the S–H bond is replaced by the stronger interaction between the oxygen atom and the ethane hydrogen atom. A low barrier (0.5 kcal mol^{-1}) also characterizes the **O1a**→**O1** isomerization.

In the **O1** $[HSO_2\cdots C_2H_5]^{\bullet+}$ species the C–H bond of C_2H_6 is significantly elongated (1.428 Å) and a new O–H bond is formed (1.197 Å). Notably, in all **O1** conformers the charge is mainly localized on the HSO_2 moiety although the ionization energy would favor C_2H_5 (see Table 2). As the formation of **O1** represents the C–H activation step, the potential energy surface was scanned by variation of the C–O versus C–H bond lengths to ascertain whether a saddle point involving hydrogen transfer to $SO_2^{\bullet+}$ can be found from the reactants to **O1** (or other conformers). No saddle points were located, which suggested a direct hydrogen-atom abstraction by the radical cation. In agreement with this is also the formation of **O1a** from the encounter complex **S1**.

Figure 5 reports the minima **O2**, **O3**, and **O4** relevant to the second activation step. The **O1** ion is not stable towards the isomerization to **O2** (Figure 6), from which it is separated by a low barrier of 2.5 kcal mol^{-1}. **O2** is the most stable ion ($\Delta H° = -81.7$ kcal mol^{-1}), with a C–O bond of 1.507 Å between the OH group of HSO_2 and the carbon atom of C_2H_5. As a result, the charge is equally distributed between HSO_2 and C_2H_5, whereas the spin is essentially localized on HSO_2. The coordination of the second hydrogen atom occurs by overcoming another barrier, still below the energy of the reactants, to give ion **O3** (Figure 6). This step eventually leads to complete charge and spin separation; ion **O3** is best described as a $[HSO_2^{\bullet}\cdots HCH_2CH_2^+]$ complex with the ethyl cation in the non-classical form.[12] A negligi-

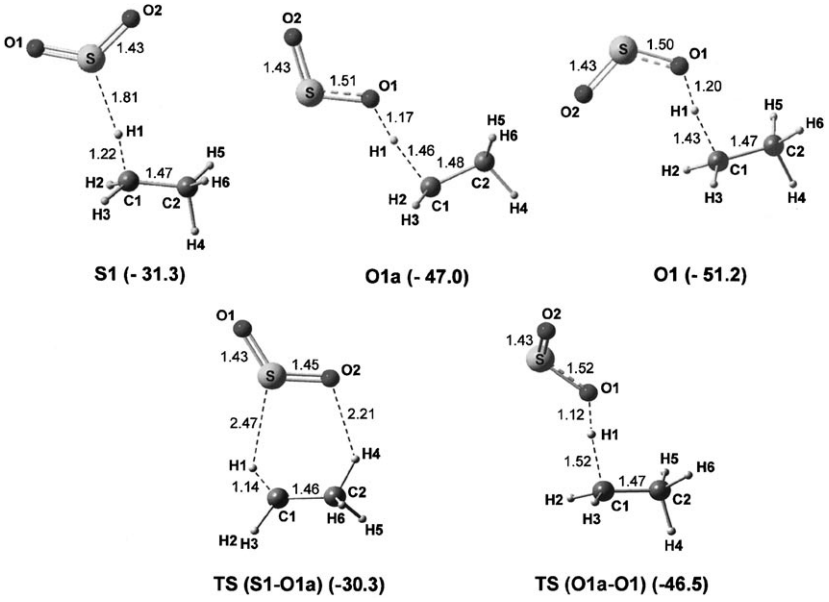

Figure 4. Geometries of the **S1**, **O1a**, and **O1** species, **TS(S1–O1a)** and **TS(O1a–O1)** transition states optimized at the PBE0//6-311G(d,p) level of theory. In parentheses, $\Delta H°$ values [kcal mol^{-1}] at 298 K relative to the reactants ($SO_2^{\bullet+} + C_2H_6$).

Table 1. Bond lengths [Å] and angles [°] of the stationary points and transition states identified along the reaction pathways **O1**→**O4** and **S1**→**O4**, $\Delta H°$ in parentheses [kcal mol^{-1}].

S1 (−31.3)	**O1a** (−47.0)	**O1** (−51.2)	**O2** (−81.7)	**O3** (−63.0)	**O4** (−70.7)
SH1 1.810	O1H1 1.174	O1H1 1.197	O1H1 0.973	O1H1 0.968	O1H1 0.975
O1S 1.434	O1S 1.505	O1S 1.504	O1S 1.901	O1H4 1.754	O2H4 1.067
O2S 1.433	O2S 1.428	O2S 1.428	O2S 1.454	O2H4 2.641	O1S 1.581
C1H1 1.222	C1H1 1.459	C1H1 1.428	C1O1 1.507	O1S 1.704	O2S 1.544
C1H2 1.093	C1H2 1.092	C1H2 1.092	C1H2 1.089	O2S 1.476	C1H2 1.087
C1H3 1.095	C1H3 1.092	C1H3 1.092	C1H3 1.091	C1H2 1.087	C1H3 1.087
C1C2 1.475	C1C2 1.479	C1C2 1.473	C1C2 1.499	C1H3 1.087	C1H4 1.835
C2H4 1.116	C2H4 1.109	C2H4 1.109	C2H4 1.091	C1H4 1.353	C1C2 1.341
C2H5 1.092	C2H5 1.093	C2H5 1.092	C2H5 1.094	C1C2 1.366	C2H4 1.830
C2H6 1.092	C2H6 1.093	C2H6 1.092	C2H6 1.094	C2H4 1.353	C2H5 1.0987
C2C1O1O2 170.9	C2C1O1O2 180	C2C1O1O2 −144.3	C2C1O1O2 −156.3	C2H5 1.087	C2H6 1.087
				C2H6 1.087	C2C1O1O2 −60.6
				C2C1O1O2 85.1	
TS(S1–O1a) (−30.3)	**TS(O1a–O1)** (−46.5)		**TS(O1–O2)** (−48.7)	**TS(O2–O3)** (−59.0)	**TS(O3–O4)** (−62.4)
SH1 2.472	O1H1 1.116		O1H1 0.995	O1H1 0.969	O1H1 0.968
SO1 1.434	SO1 1.520		C1H1 2.013	C1H4 1.153	C1H4 1.326
SO2 1.452	SO2 1.430		C1H2 1.087	C1H2 1.089	C1H2 1.087
O2H4 2.214	C1H1 1.515		C1H3 1.087	C1H3 1.089	C1H3 1.087
C1H1 1.140	C1H2 1.091		C1C2 1.452	C1C2 1.400	C1C2 1.370
C1H2 1.089	C1H3 1.092		C2H4 1.114	C2H5 1.088	C2H4 1.326
C1H3 1.113	C1C2 1.468		C2H5 1.092	C2H6 1.088	C2H5 1.087
C1C2 1.461	C1H4 1.110		C2H6 1.092	C2O2 2.994	C2H6 1.087
C2H4 1.133	C1H5 1.092		SO1 1.579	C2O1 2.585	C2O2 3.020
C2H5 1.117	C1H6 1.092		SO2 1.442	SO1 1.698	C2O1 3.345
C2H6 1.089	C2C1O1O2 −140.4		C2C1O1O2 132.4	SO2 1.476	O2H4 2.195
C2C1O1O2 20.4				C1C2O2O1 −92.9	O1H4 2.145
					SO1 1.671
					SO2 1.483
					C1C2O2O1 −86.1

ble barrier separates **O3** from **O4**, an ion–molecule complex between $H_2SO_2^{\bullet+}$ and C_2H_4, prone to dissociation into the final product $H_2SO_2^{\bullet+}$. The overall reaction is exothermic by 53.5 kcal mol^{-1}.

The reaction mechanism: Experimental and theoretical evidence demonstrates that at room temperature the $SO_2^{\bullet+}$ ions efficiently react with ethane to give the radical cation of sulfoxylic acid $H_2SO_2^{\bullet+}$ and ethylene. No intermediate is detected, even at the highest investigated pressure. The process is highly exothermic and occurs with no isotope effect, along a reaction path that lies below the reactants. The observed double C–H activation in the absence of the single C–H activation product HSO_2^+, as well as the computed charge and spin density within the intermediates, are the striking features of this reaction mechanism.

Table 2. Atomic charge and spin density in the radical ions **S1**–**O4** (PBE0//6-311G(d,p)).

Species *Moieties*	Spin	Charge
S1		
SO_2	0.434	0.470
C_2H_6	0.565	0.530
O1a		
HSO_2	0.264	0.736
C_2H_5	0.728	0.264
O1		
HSO_2	0.301	0.723
C_2H_5	0.699	0.277
O2		
HSO_2	0.999	0.491
C_2H_5	0.001	0.509
O3		
HSO_2	0.997	0.115
C_2H_5	0.003	0.885
O4		
H_2SO_2	0.966	0.777
C_2H_4	0.034	0.223

The ethane–ethylene conversion: The kinetic features of ethane–ethylene conversion are the signature of a process that depletes the reaction intermediates and leads directly to the products. In particular, the reaction of $SO_2^{\bullet+}$ with CH_3CD_3 provides specific evidence for the short lifetime of the intermediates along this path. The isotopic substitution that affects the $HDSO_2^{\bullet+}/H_2SO_2^{\bullet+}/D_2SO_2^{\bullet+}$ ratio without affecting the formation rate points to the occurrence of a partial, non-rate-determining H/D scrambling within the reaction intermediate. Notably, H/D scrambling has been observed in the dehydrogenation of ethane by ligated nickel cations, a process that leads to addition instead of loss of ethylene ($NiLC_2H_4^+ + H_2$).[7i,j]

A good candidate for the process is an ion–molecule complex containing the ethyl cation that is known to undergo intramolecular scrambling.[12] Previous work reported that the H^+/D^+ scrambling rate in isolated $C_2H_4D^+$ ions is 8.6×10^8 s^{-1} at 298 K, 3.6 times higher than in $C_2D_4H^+$ ions.[13]

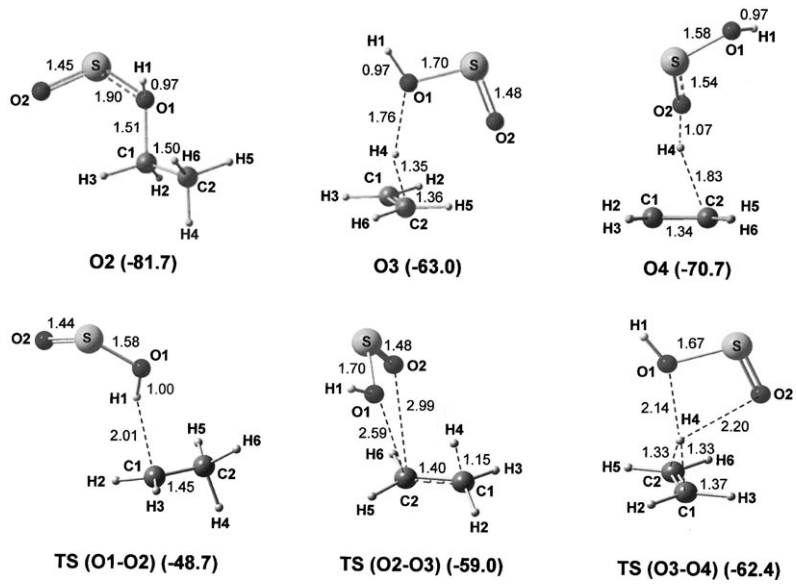

Figure 5. Geometries of species **O2–O4** and transition states **TS(O1–O2)**, **TS(O2–O3)**, and **TS(O3–O4)** optimized at the PBE0//6-311G(d,p) level of theory. In parentheses, $\Delta H°$ values [kcal mol^{-1}] at 298 K relative to the reactants ($SO_2^{\bullet+}+C_2H_6$).

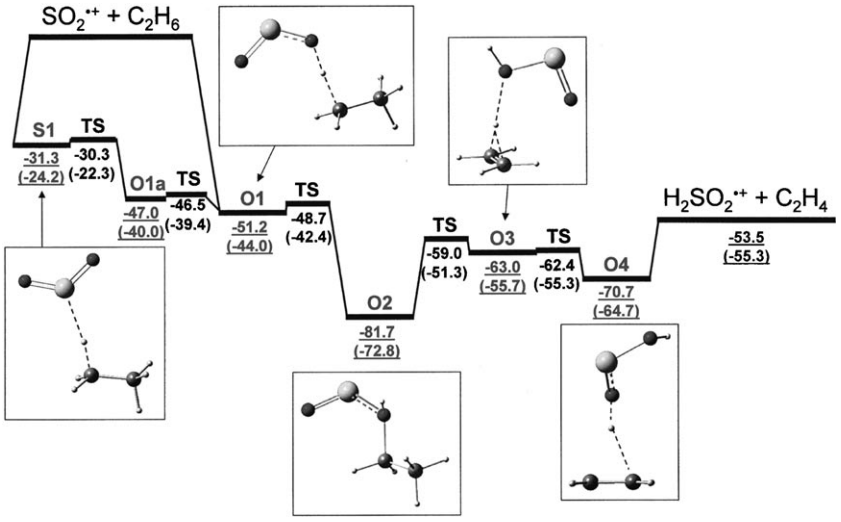

Figure 6. Simplified energy profile relevant to the ethylene-loss process ($\Delta H°$ ($\Delta G°$) in kcal mol^{-1}).

This process was used as an internal clock to evaluate the lifetime of ion–molecule complexes that contained substituted benzenes.[13] In this light, $[HSO_2^{\bullet}\cdots DCD_2CH_2^+]$ or $[DSO_2^{\bullet}\cdots HCH_2CD_2^+]$ complexes would lead to the products upon H^+ and D^+ scrambling processes that occur at different rates within the complexes. The experimental evidence indicates that the statistical ratio is not reached in the short lifetime of the intermediate, because of a sizable difference between the H^+ and D^+ scrambling rate. The intermediate converts to the products faster than it undergoes internal D^+ scrambling, which affects the H/D distribution of the products but not the reaction rate.

Consistent with these results is the transient $[HSO_2^{\bullet}\cdots HCH_2CH_2^+]$ complex **O3** predicted by the theoretical analysis. According to the profile in Figure 6, the fast conversion of **O3** into **O4** ($[H_2SO_2\cdots C_2H_4]^{\bullet+}$) efficiently competes with both the D^+ scrambling and the dissociation into $C_2H_5^+$. The barrier for the H^+ scrambling is predicted to be approximately 7 kcal mol^{-1},[12d] whereas the latter process is endothermic from **O3** by 20.6 kcal mol^{-1} and only possible at energies above the exit channel to $H_2SO_2^{\bullet+}$ (Figure 6, Table 3). It cannot be excluded that a fraction of $C_2H_5^+$ escapes, whereas the competition is expected to be much more severe for higher-energy exit channels (to HSO_2^+ and $C_2H_4^{\bullet+}$, see Table 3), as illustrated in the next paragraphs.

The formation of $C_2H_5^+$ and $C_2H_4^{\bullet+}$: Table 3 reports the thermochemistry of the reactions of formation of $C_2H_5^+$, which lead to either $H^{\bullet}+SO_2$ or $HSO_2^{\bullet}$, and of the reactions of formation of $C_2H_4^{\bullet+}$, which lead to either H_2+SO_2 or H_2SO_2, respectively. The $\Delta H°$ values of the two paths are almost equivalent in the case of $C_2H_4^{\bullet+}$, whereas the formation of $C_2H_5^+ +HSO_2^{\bullet}$ is very exothermic compared with the slightly endothermic dissociative charge transfer. Notably, the absence of the "exothermic" product HSO_2^+ ($\Delta H° = -21.3$ kcal mol^{-1}) indicates that any

Table 3. Calculated (PBE0//6-311G(d,p), 298 K) and experimental[a] $\Delta H°$ of the most relevant reactions [kcal mol^{-1}].

	Calculated	Experimental
reactants		
$SO_2^{\bullet+}/C_2H_6$	0.0	–
products		
$C_2H_6^{\bullet+}+SO_2$	−23.3	−19.1
$C_2H_5^+ +H^{\bullet}+SO_2$	+4.8	+3.0
$C_2H_5^+ +HSO_2^{\bullet}$	−42.4	–
$C_2H_4^{\bullet+}+H_2+SO_2$	−7.3	−9.8
$C_2H_4^{\bullet+}+H_2SO_2$	−7.4	–
$HSO_2^+ +C_2H_5^{\bullet}$	−22.5	−21.3
$H_2SO_2^{\bullet+}+C_2H_4$	−53.5	–

[a] From ref. [6], using thermochemical cycles for not available enthalpies of formation.

$[HSO_2\cdots C_2H_5]^{\bullet+}$ transient intermediate, amenable to dissociation into HSO_2^+, is rapidly depleted by more effective competing reactions. As anticipated, this competition may be less effective with the more exothermic formation of $C_2H_5^+$. In contrast, the formation of $C_2H_4^{\bullet+}$ by dissociation of the intermediate $[H_2SO_2\cdots C_2H_4]^{\bullet+}$, which also leads to $H_2SO_2^{\bullet+}$, is unlikely because the formation rate of $C_2H_4^{\bullet+}$ is sensitive to isotopic substitution, whereas the opposite is true for $H_2SO_2^{\bullet+}$. Also, the reaction of $SO_2^{\bullet+}$ with CH_3CD_3 only gives $C_2H_2D_2^{\bullet+}$, whereas the $HDSO_2^{\bullet+}/H_2SO_2^{\bullet+}/D_2SO_2^{\bullet+}$ ions are scrambled. This finding strongly suggests the occurrence of a different reaction path, that is, dissociative charge transfer, which competes at a stage prior to dissociation.

It has been shown that some electron coupling occurs within the encounter complex $[SO_2\cdots C_2H_6]^{\bullet+}$, though a wide range of electron transfers (ETs) can exist between the two extremes idealized as outer- and inner-sphere ET.[14] Charge transfer is therefore likely to occur at the entrance channel ($\Delta H° = -19$ kcal mol^{-1}); the $C_2H_6^{\bullet+}$ carbocation is formed with excess energy and it may undergo dissociation. In particular, the dissociation into $C_2H_4^{\bullet+}$ is characterized by a kinetic barrier of 1 eV, which is penetrated by tunneling at 0.5 eV.[15] The process is marked by a steep rise of the rate constant with the excess energy of $C_2H_6^{\bullet+}$, which becomes much larger than 10^4 s^{-1} at the internal energy of around 13 kcal mol^{-1}.[15a] In the absence of collisional stabilization, transient $[C_2H_6^{\bullet+}]^*$ ions cannot lose the excess energy before dissociation and accordingly $C_2H_6^{\bullet+}$ is only observed at high pressure. Fast unimolecular decomposition also accounts for the higher $C_2H_4^{\bullet+}$ branching ratio observed at low pressure. These processes, although fast primary reactions, are slower than the ethylene loss due to these thermochemical and kinetic requirements.

The first C–H activation: At the entrance channel of the reaction, the ion-induced dipole potential makes attractive the interaction within the $[SO_2\cdots C_2H_6]^{\bullet+}$ encounter complex **S1**. This is close to a charge-transfer complex and reflects the reactivity of $SO_2^{\bullet+}$, which coordinates C_2H_6 through the sulfur atom carrying all the positive charge.[4a] Notably, when $SO_2^{\bullet+}$ approaches C_2H_6 by the oxygen atom, the reaction leads directly to **O1** with no encounter complex and no activation barrier. In addition, **S1** easily isomerizes to **O1a-O1**. Accordingly, the direct formation of **O1** from $SO_2^{\bullet+}$ and C_2H_6, as well as its formation from **S1**, suggest that the first C–H activation is best described as a hydrogen-coupled ET from C_2H_6 to the $SO_2^{\bullet+}$ radical cation.

The second C–H activation: The first C–H activation product $[HSO_2\cdots C_2H_5]^{\bullet+}$ (**O1**) has more than 70% of the charge localized on the HSO_2 moiety despite the fact that C_2H_5 would be the energetically favored site. The charge transfer to C_2H_5 actually requires geometry changes to go from the ethyl radical to the cation. Therefore, the charge transfer occurs through the subsequent **O1**→**O3** process, which is the inner-sphere ET from $C_2H_5^{\bullet}$ to HSO_2^+ involving a geometry change.[14] In ion **O1** the hydrogen atom collinear to the O and C atoms forces the C_2H_5 group into the classical geometry of the radical, whereas in ion **O3** ($[HSO_2^{\bullet}\cdots HCH_2CH_2^+]$) the C_2H_5 group has the non-classical geometry of the cation. In **O3** charge and spin are eventually separated and the final step is a proton transfer from the ethyl cation to $HSO_2^{\bullet}$. Notably, although **O3** is located in a very shallow minimum, the occurrence of inner-sphere ET appears to be substantiated by the **O1** and **O3** ions present on the surface as $[A^+\cdots B]$ and $[A\cdots B^+]$ distinct minima rather than resonance structures.[14e] Accordingly, the second C–H activation is best described as an inner-sphere ET followed by a proton transfer.

In summary, the formation of $H_2SO_2^{\bullet+}$ proves to be a two-electron process, the first step of which occurs by hydrogen-coupled ET ($1e^-$) and the second step by inner-sphere ET followed by H^+ transfer ($1e^-$). The hydrogen-atom abstraction product HSO_2^+ is not detected as a result of the competition between two reactions sharing the same intermediate $[HSO_2\cdots C_2H_5]^{\bullet+}$: the dissociation into HSO_2^+ and the second C–H activation (computed $\Delta H°$ from the reactants $= -22.5$ and -53.5 kcal mol^{-1}, Table 3). The latter is the thermodynamically favored channel, although entropically less favored, and is characterized by very low barriers that are far below the dissociation channel. As a consequence, the ethylene-loss process rapidly depletes the $[HSO_2\cdots C_2H_5]^{\bullet+}$ intermediate, as well as the $[HSO_2\cdots HCH_2CH_2]^{\bullet+}$ and $[H_2SO_2\cdots C_2H_4]^{\bullet+}$ species. Notwithstanding, the structural features and the charge and spin distribution of the ion–molecule complexes (i.e., those containing the ethyl radical and the ethyl cation, respectively) show the crucial role of short-lived intermediates in the ET processes that underlie the double C–H activation of ethane.

Conclusion

The reaction between $SO_2^{\bullet+}$ and C_2H_6 yields $H_2SO_2^{\bullet+}$ and ethylene as the major products, both under low- (10^{-8} Torr) and high-pressure (10^{-3} Torr) regimes. The reaction is characterized by the rate constant $k = 1.0\times10^{-9}$ cm^3 s^{-1} molecule^{-1} under single-collision conditions and $k = 8.6\times10^{-10}$ cm^3 s^{-1} molecule^{-1} under multiple-collision conditions. The theoretical analysis indicates that the first C–H activation step is best described as a hydrogen-coupled ET from C_2H_6, even if the ionization energies of the alkane/SO_2 couple allow charge transfer within the initial complex. This latter process plays a greater part in $[HE\cdots H_{2n+1}C_n]^{\bullet+}$ complexes (E = electrophile, $n = 1,2$) in which, in the case of $n = 2$, it is the ethyl cation that transfers H^+ to the HSO_2 radical. The reported double C–H activation is therefore described as a multistep process involving hydrogen-coupled ET, inner-sphere ET, and H^+ transfer.

Experimental Section

FT-ICR experiments: The experiments were performed using an EXTREL FTMS 2001 double-cell mass spectrometer, equipped with a MKS ion gauge controller type 290 and modified electronic and operative systems by IONSPEC Corporation. The $SO_2^{\bullet+}$ ions were generated in the "source cell" by electron impact (200 ms, 30 eV) of the neutral SO_2 admitted into the cell at the pressure of 7.2×10^{-7} Torr. After a cooling period of 2.3 s, the $SO_2^{\bullet+}$ ions were isolated by using an "arbitrary wave-form" procedure and transferred to the "analyzer cell" that contained C_2H_6 (or C_2D_6 or CH_3CD_3). The hydrocarbons were introduced through a two-step liquid nitrogen trap to eliminate water traces. They were admitted into the analyzer cell at stationary pressures ranging from 1.5 to 3.1×10^{-8} Torr. The background H_2O in the analyzer cell was below the detection limit and no products from the very effective reaction with $SO_2^{\bullet+}$ were detected, which warranted the hydrocarbon gases as the only hydrogen-containing species. The background pressure of SO_2, which came from the source cell, was very low (2×10^{-9} Torr). Consistent with this, the thermoneutral charge transfer from $SO_2^{\bullet+}$ to SO_2, monitored by detection of $^{34}SO_2^{\bullet+}$, was negligible. Likewise, the background pressure of oxygen was low (6×10^{-9} Torr) and $O_2^{\bullet+}$ was never observed during the kinetic courses.

The pressure calibration was carried out using the rate constant value for the reference reaction $CH_4^{\bullet+}+CH_4\rightarrow CH_5^{+}+CH_3^{\bullet}$ ($k=1.1\times10^{-9}$ ($\pm15\%$) $cm^3s^{-1}molecule^{-1}$)[8] and the reading was further corrected for the individual response factors of CH_4 and C_2H_6.[16] The $SO_2^{\bullet+}$ intensities fit pseudo-first order kinetics $c=c_0e^{-k_{obs}t}$ (c is the ion intensity at time t, k_{obs} is the pseudo-unimolecular decay rate constant). The product intensities fit the equation $c=(k_f/k_{obs})c_0(1-e^{-k_{obs}t})$; k_f is the pseudo-unimolecular growth rate constant of a given product. The branching ratios were obtained by k_f/k_{obs} with a precision of $\leq10\%$. The bimolecular rate constants k ($cm^3s^{-1}molecule^{-1}$) were obtained by k_{obs} (or k_f) and the neutral reactant density; the accuracy of the bimolecular rate constants was evaluated at $\pm30\%$ because of the uncertainties that arise for the most part from the measurement of the neutral pressure.[3e] The reaction efficiency, expressed as the ratio of the bimolecular rate constant k to the collision rate constant, was calculated according to the ADO theory.[17]

ITMS experiments: The experiments were performed with a LTQ XL linear quadrupole ion-trap mass spectrometer (Thermo Fischer Scientific), equipped with an atmospheric pressure chemical ionization source (API-CI). N_2 was used as the sheath and auxiliary gas. Typical experimental conditions were as follows: flow rate = 20 and 5 arbitrary units for the sheath and auxiliary gas, respectively (a.u. $\approx$ 0.37 L min^{-1});[18] discharge current = 3–4 μA; capillary and vaporizer temperature = 150 and 30 °C, respectively.

The instrument was partially modified to allow the introduction of reagent gases into the vacuum chamber. To this end, the rear plate of the instrument was replaced by a custom-made plate with a 6.25 mm hole with a peek tube of 0.75 mm internal diameter (i.d.) inside. The peek tube enters the vacuum region and contains two deactivated fused-silica capillaries of 0.25 mm i.d., through which the neutral gases can be introduced separately. The capillaries are positioned coaxially to the rear hole of the trap, which typically allows the use of ETD or Orbitrap manifolds.

The pressure of the buffer gas (helium) was measured by a Pirani APG-L gauge (Edwards), connected to a Teflon tube (4 mm i.d.) passing through the hole of the rear plate and just in contact with the metal plate of the trap, close to the helium entrance. The measured pressure was 2.9×10^{-3} ($\pm15\%$) Torr, in agreement with available data for linear quadrupole ion traps.[19] The pressure of the neutral gases introduced into the trap was kept constant by a Granville–Phillips leak valve and measured by a Granville–Phillips Series 370 Stabil Ion Vacuum Gauge (accuracy $\pm4\%$ of reading). The readings were calibrated using the known rate constants of ion–molecule reactions performed by FT-ICR, guided ion beam (GIB), and SIFT mass spectrometers. The reactions of Pt^+ and FeO^+ with CH_4 were used as the reference reactions[3e,20] and the readings were further corrected for individual response factors of the neutral reactants.[16]

In a typical kinetic experiment, a limited amount of SO_2 was introduced into the chamber and ionized by charge exchange from $N_2^{\bullet+}$ ions formed in the atmospheric pressure source.[21] The $SO_2^{\bullet+}$ ions were then thermalized by thousands of collisions (collision frequency $\approx10^5$ s^{-1}) with the buffer gas ($t\leq0.1$ s),[22] isolated, and allowed to react with the neutral substrate C_2H_6. This was introduced into the trap (through a liquid nitrogen trap) at pressures ranging from 7×10^{-8} to 5×10^{-7} Torr. Mass spectra were recorded at each reaction time in full-scan mode, with injection time = 10 ms, collision energy = 0 eV, and the activation parameter Q optimized to ensure stable trapping fields for the expected products. Each spectrum represents the average of 20 scans, recorded with a minimum of three replicates for each kinetic run, and 3–10 kinetic runs for each pressure of C_2H_6. Xcalibur 2.0.6 software was used for data acquisition and processing.

To evaluate the water background the following procedure was followed. Two effective ion–molecule reactions were used to titrate the water content into the trap, the reactions of $Ar^{\bullet+}$ ($k=1.6\times10^{-9}$ ($\pm20\%$) $cm^3s^{-1}molecule^{-1}$)[8] and $SO_2^{\bullet+}$ ($k=2.6\times10^{-9}$ ($\pm30\%$) $cm^3s^{-1}molecule^{-1}$).[4b] The $Ar^{\bullet+}$ ions were produced by corona discharge of argon (discharge current = 0.5–0.6 μA), introduced in the APCI source through the sheath and auxiliary lines usually used for nitrogen gas. They were isolated and made to react with the water background. The water density value can be obtained by k_{obs}/k (k_{obs} is the observed pseudo-unimolecular rate constant and k is the known second-order rate constant). A number of experiments performed under different experimental conditions and on different days gave water density values that varied from 2.2–2.9×10^9 molecules cm^{-3}, which correspond to water partial pressures of 6.8–9.0×10^{-8} Torr. In the second reaction, the $SO_2^{\bullet+}$ ions were produced as described above and made to react with the water background. The reaction was recorded in approximately 70 kinetic runs and the observed rate constants $k_{obs(water)}$ ranged from 5.1–6.6 s^{-1}, dependent on the variable day-to-day pressure of water. From $k_{obs(water)}$ and the known second-order rate constant, we obtained water density values ranging from 2.0–2.5×10^9 molecules cm^{-3}, in good agreement with the results obtained from the $Ar^{\bullet+}$ reaction.

To minimize errors in the reaction between $SO_2^{\bullet+}$ and C_2H_6, the reaction of $SO_2^{\bullet+}$ with the background was recorded before each kinetic run. The k_{obs} value of the reaction with C_2H_6 was therefore corrected for $k_{obs(water)}$ measured in each specific run. Figure 2B reports the plot of the corrected k_{obs} values as a function of the C_2H_6 density and shows a very good correlation coefficient. It also shows that the bimolecular rate constant k, obtained by the corrected k_{obs} and the C_2H_6 neutral density, does not vary with C_2H_6 density. The procedure was conclusively verified by the reaction of $SO_2^{\bullet+}$ with CH_4, the measured rate constant ($k=6.48\times10^{-10}$ ($\pm30\%$) $cm^3s^{-1}molecule^{-1}$) is in very good agreement with the reported value of 6.58×10^{-10}($\pm30\%$) $cm^3s^{-1}molecule^{-1}$.[4a] All the examined reactions displayed a pseudo-first-order decay, verified by the logarithmic plots of the reactant ions concentrations versus time.

Materials: All chemicals were research-grade products purchased from Aldrich with a stated purity in excess of 99.9 mol%. C_2D_6 (99 atom%) and CH_3CD_3 (99 atom%) were purchased from Isotec and Icon Isotopes, respectively.

Computational methods: All calculations were performed by the Gaussian 03 package[23] by using a well-tested hybrid density functional (PBE0),[24] with a triple-zeta polarized basis set (6-311G(d,p))[25]), to analyze the structure, relative stability, and harmonic force field of all the stationary points located on the potential energy surface (PES). From these data, enthalpies and Gibbs free energies at 298 K have been evaluated by standard statistical thermodynamics equations for an ideal gas within the harmonic oscillator-rigid rotor approximation. The choice of the computational method has been first validated by comparison with the experimental values available for some of the most significant products (see Table 3). Although not perfect, the agreement between experimental and computed values is sufficient to guarantee a reliable analysis of general trends and a safe comparison between different pathways.

Acknowledgements

Financial support by the Italian Government (PRIN) and Rome University "La Sapienza" is gratefully acknowledged. The authors thank Stefania Recaldin for editorial assistance.

[1] a) G. A. Olah, *Acc. Chem. Res.* **1987**, *20*, 422; b) J. Sommer, J. Bukala, *Acc. Chem. Res.* **1993**, *26*, 370; c) D. Schröder, H. Schwarz, *Angew. Chem.* **1995**, *107*, 2126; *Angew. Chem. Int. Ed. Engl.* **1995**, *34*, 1973; d) J. J. Schneider, *Angew. Chem.* **1996**, *108*, 1132; *Angew. Chem. Int. Ed. Engl.* **1996**, *35*, 1068; e) A. E. Shilov, G. B. Shul'pin, *Chem. Rev.* **1997**, *97*, 2879; f) S. S. Stahl, J. A. Labinger, J. E. Bercaw, *Angew. Chem.* **1998**, *110*, 2298; *Angew. Chem. Int. Ed.* **1998**, *37*, 2180; g) R. A. Periana, D. J. Taube, S. Gamble, H. Taube, T. Satoh, H. Fujii, *Science* **1998**, *280*, 560; h) R. H. Crabtree, *J. Chem. Soc. Dalton Trans.* **2001**, 2437; i) A. A. Fokin, P. R. Schreiner, *Chem. Rev.* **2002**, *102*, 1551; j) A. A. Fokin, T. E. Shubina, P. A. Gunchenko, S. D. Isaev, A. G. Yurchenko, P. R. Schreiner, *J. Am. Chem. Soc.* **2002**, *124*, 10718; k) J. A. Labinger, *J. Mol. Catal. A* **2004**, *220*, 27; l) D. K. Böhme, H. Schwarz *Angew. Chem.* **2005**, *117*, 2388; *Angew. Chem. Int. Ed.* **2005**, *44*, 2336; m) D. Schröder, H. Schwarz, *Proc. Natl. Acad. Sci. USA* **2008**, *105*, 18114; n) R. H. Crabtree, *Nat. Chem.* **2009**, *1*, 348.

[2] a) G. A. Olah, H. C.-H. Lin, *J. Am. Chem. Soc.* **1971**, *93*, 1259; b) G. A. Olah, P. Schilling, *J. Am. Chem. Soc.* **1973**, *95*, 7680; c) G. A. Olah, N. Hartz, G. Rasul, Q. Wang, G. K. S. Prakash, J. Casanova, K. O. Christe, *J. Am. Chem. Soc.* **1994**, *116*, 5671; d) F. Cacace, G. de Petris, F. Pepi, M. Rosi, A. Troiani, *Chem. Eur. J.* **1999**, *5*, 2750; e) G. de Petris, F. Pepi, M. Rosi, *Chem. Phys. Lett.* **1999**, *304*, 191; f) D. J. Levandier, Y.-H. Chiu, R. A. Dressler, L. Sun, G. C. Schatz, *J. Phys. Chem. A* **2004**, *108*, 9794; g) F. Pepi, A. Tata, S. Garzoli, M. Rosi, *Chem. Phys. Lett.* **2008**, *461*, 21.

[3] a) K. K. Irikura, J. L. Beauchamp, *J. Am. Chem. Soc.* **1991**, *113*, 2769; b) D. Schröder, A. Fiedler, J. Hrušák, H. Schwarz, *J. Am. Chem. Soc.* **1992**, *114*, 1215; c) P. A. M. van Koppen, P. R. Kemper, J. F. Bushnell, M. T. Bowers, *J. Am. Chem. Soc.* **1995**, *117*, 2098; d) M. Pavlov, M. R. A. Blomberg, P. E. M. Siegbahn, R. Wesendrup, C. Heinemann, H. Schwarz, *J. Phys. Chem. A* **1997**, *101*, 1567; e) D. Schröder, H. Schwarz, D. E. Clemmer, Y. Chen, P. B. Armentrout, V. Baranov, D. K. Bohme, *Int. J. Mass Spectrom. Ion Proc.* **1997**, *161*, 175; f) X.-G. Zhang, R. Liyanage, P. B. Armentrout, *J. Am. Chem. Soc.* **2001**, *123*, 5563; g) Q. Zhang, M. T. Bowers, *J. Phys. Chem. A* **2004**, *108*, 9755; h) F.-X. Li, P. B. Armentrout, *J. Chem. Phys.* **2006**, *125*, 133114; i) S. Feyel, J. Döbler, D. Schröder, J. Sauer, H. Schwarz, *Angew. Chem.* **2006**, *118*, 4797; *Angew. Chem. Int. Ed.* **2006**, *45*, 4681; j) M. Schlangen, H. Schwarz, *Angew. Chem.* **2007**, *119*, 5711; *Angew. Chem. Int. Ed.* **2007**, *46*, 5614; k) S. Feyel, J. Döbler, R. Höckendorf, M. K. Beyer, J. Sauer, H. Schwarz, *Angew. Chem.* **2008**, *120*, 1972; *Angew. Chem. Int. Ed.* **2008**, *47*, 1946; l) A. Shayesteh, V. V. Lavrov, G. K. Koyanagi, D. K. Bohme, *J. Phys. Chem. A* **2009**, *113*, 5602.

[4] a) G. de Petris, A. Troiani, M. Rosi, G. Angelini, O. Ursini, *Chem. Eur. J.* **2009**, *15*, 4248; b) G. de Petris, A. Cartoni, A. Troiani, G. Angelini, O. Ursini, *Phys. Chem. Chem. Phys.* **2009**, *11*, 9976.

[5] N. Dietl, M. Engeser, H. Schwarz, *Angew. Chem.* **2009**, *121*, 4955; *Angew. Chem. Int. Ed.* **2009**, *48*, 4861.

[6] NIST Chemistry WebBook, NIST Standard Reference Database Number 69 (Eds.: P. J. Linstrom, W. G. Mallard), Gaithersburg, **2005**, http://webbook.nist.gov.

[7] a) L. Sunderlin, N. Aristov, P. B. Armentrout, *J. Am. Chem. Soc.* **1987**, *109*, 78; b) K. Eller, H. Schwarz, *Chem. Rev.* **1991**, *91*, 1121; c) D. Schröder, H. Schwarz, *Angew. Chem.* **1991**, *103*, 987; *Angew. Chem. Int. Ed. Engl.* **1991**, *30*, 991; d) A. Sen, M. A. Benvenuto, M. Lin, A. C. Hutson, N. Basickes, *J. Am. Chem. Soc.* **1994**, *116*, 998; e) M. C. Holthausen, A. Fiedler, H. Schwarz, W. Koch, *J. Phys. Chem.* **1996**, *100*, 6236; f) I. Kretzschmar, A. Fiedler, J. N. Harvey, D. Schröder, H. Schwarz, *J. Phys. Chem. A* **1997**, *101*, 6252; g) D. Zhang, C. Liu, S. Bi, S. Yuan, *Chem. Eur. J.* **2003**, *9*, 484; h) D. J. Levandier, Y-H. Chiu, R. A. Dressler, *J. Chem. Phys.* **2004**, *120*, 6999; i) M. Schlangen, D. Schröder, H. Schwarz, *Chem. Eur. J.* **2007**, *13*, 6810; j) M. Schlangen, H. Schwarz, D. Schröder, *Helv. Chim. Acta* **2007**, *90*, 847; k) P. B. Armentrout, *Organometallics* **2007**, *26*, 5473; l) P. B. Armentrout, *Organometallics* **2007**, *26*, 5486.

[8] V. G. Anicich, *J. Phys. Chem. Ref. Data* **1993**, *22*, 1469.

[9] N. Dietl, M. Engeser, H. Schwarz, *Chem. Eur. J.* **2009**, *15*, 11100.

[10] S. Gronert, *Mass Spectrom. Rev.* **2005**, *24*, 100.

[11] a) D. Schröder, R. Brown, P. Schwerdtfeger, H. Schwarz, *Int. J. Mass Spectrom.* **2000**, *203*, 155; b) S. Le Caër, M. Heninger, P. Pernot, H. Mestdagh, *Phys. Chem. Chem. Phys.* **2002**, *4*, 1855.

[12] a) P. Ausloos, R. E. Rebbert, L. W. Sieck, T. O. Tiernan, *J. Am. Chem. Soc.* **1972**, *94*, 8939; b) F. A. Houle, L. Beauchamp, *J. Am. Chem. Soc.* **1979**, *101*, 4067; c) K. Raghavachari, R. A. Whiteside, J. A. Pople, P. von R. Schleyer, *J. Am. Chem. Soc.* **1981**, *103*, 5649; d) H.-S. Andrei, N. Solcà, O. Dopfer, *Angew. Chem.* **2008**, *120*, 401; *Angew. Chem. Int. Ed.* **2008**, *47*, 395.

[13] M. Aschi, M. Attinà, F. Cacace, *Chem. Eur. J.* **1998**, *4*, 1535.

[14] a) A. Haim, *Acc. Chem. Res.* **1975**, *8*, 264; b) J. K. Kochi, *Acc. Chem. Res.* **1992**, *25*, 39; c) M. Patz, S. Fukuzumi, *J. Phys. Org. Chem.* **1997**, *10*, 129; d) S. M. Hubig, R. Rathore, J. K. Kochi, *J. Am. Chem. Soc.* **1999**, *121*, 617; e) D. Schröder, C. Trage, H. Schwarz, D. Danovich, S. Shaik, *Int. J. Mass Spectrom.* **2000**, *200*, 163.

[15] a) K.-M. Weitzel, *Int. J. Mass Spectrom. Ion Proc.* **1994**, *136*, 1; b) T. Baer, *Int. J. Mass Spectrom.* **2000**, *200*, 443.

[16] J. E. Bartmess, R. M. Georgiadis, *Vacuum* **1983**, *33*, 149.

[17] M. T. Bowers, T. Su, *Interactions between Ions and Molecules*, Plenum Press, New York, **1975**.

[18] C. M. Leavitt, V. S. Bryantsev, W. A. de Jong, M. S. Diallo, W. A. Goddard III, G. S. Groenewold, M. J. Van Stipdonk, *J. Phys. Chem. A* **2009**, *113*, 2350.

[19] J. C. Schwartz, M. W. Senko, J. E. P. Syka, *J. Am. Soc. Mass Spectrom.* **2002**, *13*, 659.

[20] D. Schröder, H. Schwarz, *Can. J. Chem.* **2005**, *83*, 1936.

[21] The energy from charge transfer at thermal collision energy is partitioned between the $SO_2^{\bullet+}$ and N_2 products, also considering the absence of $SO_2^{\bullet+}$ states between 14 and 16 eV. See: a) R. Marx, G. Mauclaire, R. Derai, *Int. J. Mass Spectrom. Ion Proc.* **1983**, *54–55*, 155; b) L. Wang, Y. T. Lee, D. A. Shirley, *J. Chem. Phys.* **1987**, *87*, 2489.

[22] For the average energies transferred per collision of neutral SO_2* with He, to be taken as a conservative lower limit, see: M. Heymann, H. Hippler, D. Nahr, H. J. Plach, J. Troe, *J. Phys. Chem.* **1988**, *92*, 5507.

[23] Gaussian 03, Revision D.02, M. J. Frisch, G. W. Trucks, H. B. Schlegel, G. E. Scuseria, M. A. Robb, J. R. Cheeseman, J. A. Montgomery, Jr., T. Vreven, K. N. Kudin, J. C. Burant, J. M. Millam, S. S. Iyengar, J. Tomasi, V. Barone, V. Mennucci, M. Cossi, G. Scalmani, N. Rega, G. A. Petersson, H. Nakatsuji, M. Hada, M. Ehara, K. Toyota, R. Fukuda, J. Hasegawa, M. Ishida, T. Nakajima, Y. Honda, O. Kitao, H. Nakai, M. Klene, X. Li, J. E. Knox, H. P. Hratchian, J. B. Cross, C. Adamo, J. Jaramillo, R. Gomperts, R. E. Stratmann, O. Yazyev, A. J. Austin, R. Cammi, C. Pomelli, J. W. Ochterski, P. J. Ayala, K. Morokuma, G. A. Voth, P. Salvador, J. J. Dannenberg, V. G. Zakrewski, S. Dapprich, A. D. Daniels, M. C. Strain, O. Farkas, D. K. Malick, A. D. Rabuck, K. Raghavachari, J. B. Foresman, J. V. Ortiz, Q. Cui, A. G. Baboul, S. Clifford, J. Cioslowski, B. B. Stefanov, G. Liu, A. Liashenko, P. Piskorz, I. Komaromi, R. L. Martin, D. J. Fox, T. Keith, M. A. Al-Laham, C. Y. Peng, A. Nanayakkara, M. Challacombe, P. M. W. Gill, B. Johnson, W. Chen, M. W. Wong, C. Gonzalez, J. A. Pople, Gaussian, Inc., Wallingford, CT, **2004**.

[24] C. Adamo, V. Barone, *J. Chem. Phys.* **1996**, *104–105*, 158.

[25] K. Raghavachari, J. S. Binkley, R. Seeger, J. A. Pople, *J. Chem. Phys.* **1980**, *72*, 650.

Received: December 31, 2009
Revised: March 8, 2010
Published online: April 21, 2010

